Annu. Rev. Phys. Chem. 2003. 54:141–72
doi: 10.1146/annurev.physchem.54.011002.103811

First published online as a Review in Advance on January 8, 2003

CONJUGATED POLYMERS AS MOLECULAR MATERIALS: How Chain Conformation and Film Morphology Influence Energy Transfer and Interchain Interactions

Benjamin J. Schwartz
Department of Chemistry and Biochemistry, University of California, Los Angeles, California 90095-1569; email: schwartz@chem.ucla.edu

Key Words poly(phenylene vinylene) and derivatives, excimer, aggregate, LED, spectroscopy

■ **Abstract** The electronic structure of conjugated polymers is of current interest because of the wide range of potential applications for such materials in optoelectronic devices. It is increasingly clear that the electronic properties of conjugated polymers depend sensitively on the physical conformation of the polymer chains and the way the chains pack together in films. This article reviews the evidence that interchain electronic species do form in conjugated polymer films, and that their number and chemical nature depend on processing conditions; the chain conformation, degree of interchain contact, and rate of energy transfer can be controlled by factors such as choice of solvent, polymer concentration, thermal annealing, presence of electrically charged side groups, and encapsulation of the polymer chains in mesoporous silica. Taken together, the results reconcile many contradictions in the literature and provide a prescription for the optimization of conjugated polymer film morphology for device applications.

INTRODUCTION TO CONJUGATED POLYMERS

Overview

Conjugated polymers are novel materials that combine the optoelectronic properties of semiconductors with the mechanical properties and processing advantages of plastics (1). When functionalized with flexible side groups (2), these materials become soluble in organic solvents and can be solution processed at room temperature into large-area, optical-quality thin films (3); such films are readily fabricated into desired shapes that are useful in novel devices (4). The ease of polymer processing compared with conventional inorganic semiconductors offers the potential for enormous cost-savings in applications that require visible band-gap semiconductors. Thus, conjugated polymers offer the possibility for use in devices

such as plastic LEDs (4, 5), photovoltaics (6), transistors (7), and in completely new applications such as flexible displays.

Despite this enormous versatility for optoelectronic applications, some of the fundamental physics underlying the construction or optimization of practical devices based on these materials remains controversial or poorly understood. Nearly all of this controversy stems from a lack of understanding concerning the interactions between conjugated polymer chains in high-concentration solutions or films. The main issue is that the electronic properties of conjugated polymers are often assumed to be analogous with those of traditional inorganic semiconductors. In fact, one of the standard theories for describing the electronic structure of conjugated polymers is based on a free-electron gas whose motions are coupled to vibrations of the polymer backbone (8). Although this type of picture works well for explaining many of the properties of conjugated polymers in isolation, it fails to describe the complex interactions between chains in conjugated polymer films. Thus, the central tenet of this work is that conjugated polymers are best thought of as molecular materials. A conjugated polymer film is composed of many individual polymer chains; what we argue throughout this review is that both the physical conformation of these chains and the way they pack together in a film determine many of the important optical and electronic properties that are critical to the operation of devices based on these materials. The morphology of conjugated polymer films, in turn, is controlled by the details of how the films are processed, so it is not surprising that different groups who have studied polymer films prepared in different ways have reached different and often controversial conclusions.

Excitons on Isolated Conjugated Polymer Chromophores

Figure 1 shows the chemical structure as well as the dilute-solution absorption and photoluminescence (PL) spectrum of one of the most common soluble semiconducting polymers, poly[2-methoxy-5-(2′-ethyl-hexyloxy)-1,4-phenylene vinylene] (MEH-PPV). The polymer is a bright orange color, the result of a $\pi \rightarrow \pi^*$ transition centered near 500 nm. Even for an idealized chain structure, excitation of this transition is not delocalized over the entire chain: Instead, the excitation, including its associated benzoid-to-quinoid bond-order reversal, remains localized over just a few (typically 4–10) repeat units of the backbone (9, 10). The excitation, including the associated changes in bond length along the backbone, is commonly referred to as an exciton; Brédas and coworkers have given excellent reviews offering a "translation" of the quasi-particle nomenclature for conjugated polymer electronic states into a more traditional physical chemistry language (10, 11).

Real conjugated polymer chains in solutions and films, however, do not have the ideal structure depicted in Figure 1 because they tend to twist and coil. Our "zeroth order" description of a conjugated polymer chain is that of a series of linked chromophores, each of which has a different extent of π-electron delocalization; each conjugated segment is roughly planar with its extent of conjugation limited by twists of the polymer backbone. In a simple 1D particle-in-a-box picture of electron delocalization along these segments, the longer segments will have a low

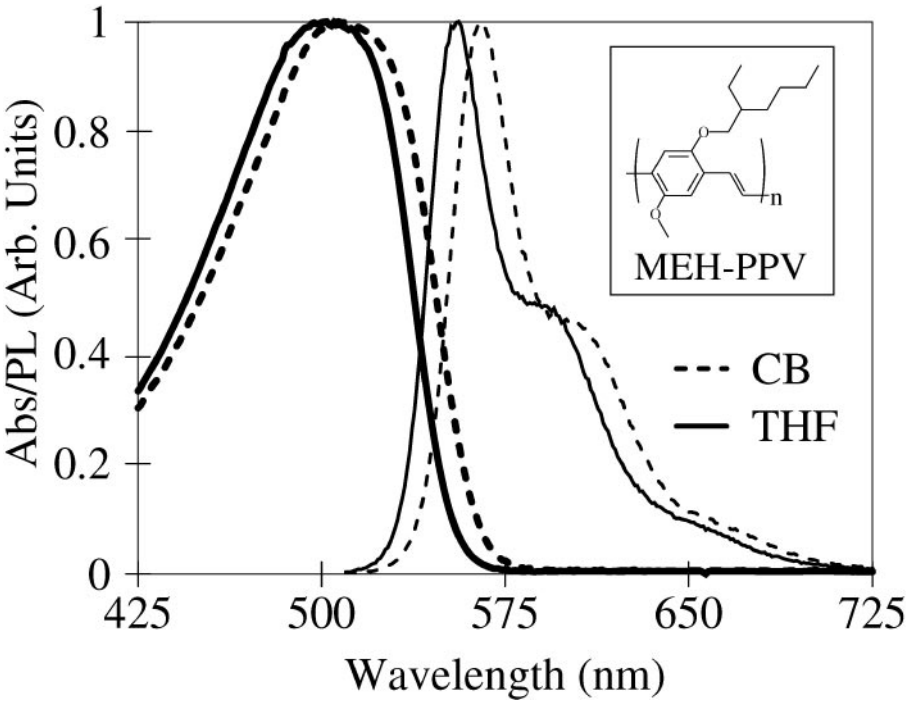

Figure 1 Normalized UV-visible absorption (*heavy curves*) and PL (*thin curves*) spectra of MEH-PPV in dilute solutions of chlorobenzene (CB, *dashed curves*) and tetrahydrofuran (THF, *solid curves*) (44). The inset shows the chemical structure of MEH-PPV.

$\pi \rightarrow \pi^*$ energy gap whereas the exciton energy of the shortest segments will be much higher. The featureless absorption spectrum consists of an inhomogeneous superposition of absorptions from segments with different conjugation lengths and thus, different energy gaps. The more structured emission spectrum, whose vibronic features reflect the excited-state displacement in the C═C stretch, is highly Stokes-shifted because excitons on high-energy segments will undergo rapid energy transfer to lower-energy segments, so that nearly all the emission comes from low energy, long conjugation length chromophores. The details of how this energy transfer process occurs will be discussed further below. We note here that this picture of energy migration through an inhomogeneous distribution of chromophores with different energies is generally [although not entirely (12)] well accepted in the literature (13–16).

A Menagerie of Possible Interchain Species

Although it is well accepted that photoexcitation of an isolated conjugated polymer chromophore produces an intrachain exciton (17–20), the picture is much less clear when adjacent chromophores π-electrons are in close proximity, enabling

the formation of interchain species. There are many ways that conjugated polymer chromophores can interact, and a great deal of terminology for describing the different possible interactions. When two adjacent polymer chromophores' share their π-electrons equally in the excited state but not in the ground state, the interchain excited state is referred to as an "excimer" (21–23). Conjugated polymers whose π-electrons are neutrally delocalized over multiple segments in both the ground and excited states are known as "aggregates" (24–26). Our definition of aggregates is photophysical: We say that polymer segments are aggregated only when the extent of π-delocalization is significantly altered from that of a single chromophore. Thus, we do not refer to agglomerated conjugated polymer chains whose chromophores do not interact electronically as aggregated. In addition to neutral electron delocalization, charge transfer can occur upon excitation of strongly interacting chromophores, leaving a radical cation, or hole polaron, on one segment and a radical anion, or electron polaron, on the other. This type of charge-separated interchain species is typically referred to as a "polaron pair" (27, 28), or occasionally as a "spatially indirect exciton" (29). Interchain excited states with an unequal sharing of π-electron density between segments or a partial degree of charge transfer character (i.e., somewhere between excimers and polaron pairs) are labeled "exciplexes" (21, 30). It is worth noting that our definition of interchain interactions implies only that π-electron density is delocalized between multiple conjugated segments; this definition does not depend on whether the interacting chromophores reside on physically distinct chains or are tethered together along the same polymer backbone. Given that there are an infinite number of ways the chains can pack in a conjugated polymer film, we expect a continuum of delocalized excited states with varying degrees of charge transfer character as well as different extents of interchain delocalization in the ground and excited states.

Controversy over Interchain Species in Conjugated Polymers

One of the primary spectral signatures of excited interchain species in conjugated polymers is a redshifted emission caused by the delocalization of the π-electrons between conjugated segments, which lowers the interchain electronic energy relative to that of the single-chain exciton. This signature emission provides only a hazy distinction between the various possible interchain species, especially considering that energy transfer can populate low-energy interchain states from higher-energy intrachain excitons. Interchain emission is not always easy to detect because the overlap of the delocalized interchain excited state with the single-chain ground state wave function is usually poor, leading to long radiative lifetimes (31). These long lifetimes, in combination with the myriad nonradiative processes available to the excited states of conjugated polymers, lead to very low quantum yields for the interchain emission, especially at room temperature (23, 27). In addition to the weak, redshifted PL, aggregates (unlike excimers and polaron pairs) are also characterized by a weak, redshifted ground state absorption between the

delocalized ground and excited states (24, 25). This low-energy aggregate absorption is often forbidden by symmetry and thus also can be hard to detect. With all these difficulties, even the fact that the spectral signatures of excimers and aggregates have been observed in some conjugated polymers (21–30) has not been enough to quell the controversy over the existence and nature of interchain species in films of these materials. Indeed, a veritable host of steady state (30, 32–35) and time-resolved (19–29) experiments have been performed on a variety of conjugated polymers, leading to literature estimates of the fraction of photoexcitations that result in interchain species ranging from essentially zero (32) to 90% (29).

Why Interchain Species are Important

The controversy over the existence and nature of interchain species is not just academic: The formation of interchain species has significant implications for charge transport and light emission in conjugated polymer-based devices. The mobility of electrical charges along the backbone of a single polymer chain in solution is quite high, approaching that of many common metals (36). In the films that form the active layer of conjugated polymer-based devices, however, the individual polymer strands are not mobile, providing no way to "heal" the twists in the chain that break the conjugation. Moreover, spin-coating tends to leave the polymer chains lying in the plane of the film (37) so that there rarely is a single polymer chain bridging the electrodes in a sandwich structure (electrode/thin polymer film/electrode) device. Thus, as we argue further below, charge transport through conjugated polymer films requires intimate electrical contact between the polymer segments.

Although interchain interactions might be beneficial to charge transport, the presence of weakly emissive interchain species would serve to significantly reduce the efficiency of electroluminescence (EL) from conjugated polymer devices. The maximum possible EL efficiency of a conjugated polymer-based device is often estimated as 25% of the PL quantum efficiency (38): The argument is based on simple spin statistics, assuming that 3 of every 4 pairs of oppositely charged carriers that recombine produce nonemissive triplet excitons, whereas only 1 in 4 create the desired emissive singlet excitons [although recently this assumption has been called into question (39–42)]. If the existence of interchain species is intrinsic, then there is no simple relationship between the PL and EL efficiencies of conjugated polymer films (43). This leaves open the question of whether or not there is significant room for improvement in the current generation of polymer light-emitting devices. Moreover, even if the interchain species in a conjugated polymer film were relatively dilute, the fact that interchain states lie at the bottom of the excited-state energy funnel guarantees they would have a significant impact on device performance: As discussed below, all the energy from nearby emissive excitons would rapidly migrate to the weakly emissive interchain states, leading to significant quenching of the luminescence.

THE SOLUTION ORIGINS OF INTERACTIONS BETWEEN CONJUGATED POLYMER CHAINS

Connection Between Solution Chain Conformation and Interchain Species

Given the importance of interchain interactions in polymer films for device performance, the most logical place to start understanding the origins of such interactions is in the study of the polymer solutions from which the films are cast. Figure 2 shows the results of dynamic light scattering (DLS) experiments on chains of MEH-PPV dissolved in both chlorobenzene (CB) and tetrahydrofuran (THF) (44). DLS measures the diffusion coefficient of the individual polymer chains in the solution, which in combination with the solution viscosity and the Stokes-Einstein relation gives the typical size (hydrodynamic radius) of the solvated polymer coil. The size distributions in Figure 2 show that in the good solvent CB, MEH-PPV chains have a relatively open and straight conformation, which is best to maximize favorable solute-solvent interactions. In the poor solvent THF, MEH-PPV chains form a much tighter coil as the polymer curls up to minimize unfavorable interactions with the solvent. This change in conformation is also

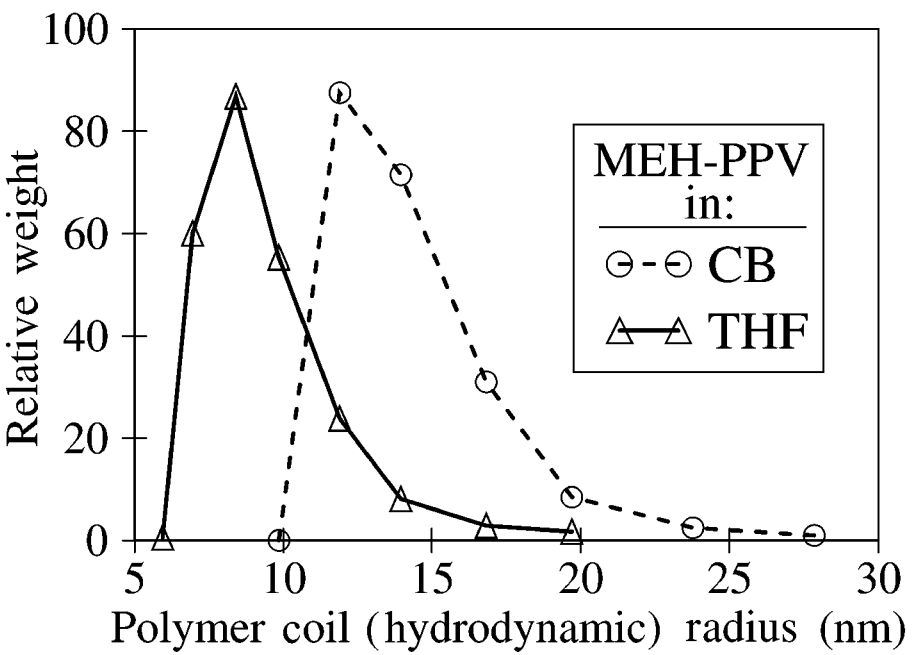

Figure 2 Size distributions (hydrodynamic radii) determined by DLS for the same solutions of MEH-PPV whose absorption and PL spectra are shown in Figure 1. The circles/dashed curve show the results for the CB solution, and the triangles/solid curve show the results for the THF solution (44). The molecular weight of the MEH-PPV is ~500,000.

reflected in the absorption and PL spectra of the polymer solutions (Figure 1): Both spectra are slightly blueshifted in THF relative to CB because the tighter chain coil in THF is produced via twisting of the polymer backbone, resulting in segments with a shorter average conjugation length (44).

In addition to the change in conformation, we also found evidence that MEH-PPV forms aggregate species with absorption and emission spectra that are distinctly redshifted from the intrachain exciton (44). Moreover, the degree of aggregation we observed depends on both the choice of solvent and the polymer concentration. Aggregation is promoted in solvents such as CB in which the chains have a relatively open coil and hindered in solvents such as THF where the chains tend to coil tightly. And, as expected, aggregation increases with increasing polymer concentration in both solvents, with aggregates comprising a significant fraction of the total number of excited state species at the concentrations typically used for spin-coating polymer films. Thus, our results suggest that the ability for conjugated polymer chromophores to interact in solution depends on their mutual accessibility: The more exposed the chromophore, the more likely it is to interact with a neighboring chromophore (44). The fact that aggregation between MEH-PPV chains in dilute solutions is promoted when the backbone is straight and hindered when the backbone is coiled suggests that aggregation is more common between chromophores on distinct chains than between chromophores on the same chain, as discussed further below. Both theoretical calculations and experiments on conjugated chromophores held in well-defined geometries suggest that π-electron contact must take place over the entire length of the exciton (several polymer repeat units) to form the electronically distinct aggregate species (45, 46). We believe that conjugated polymers are sufficiently stiff so that it is difficult to fold a chain to bring two straight conjugated segments into the parallel configuration necessary for interchain delocalization, explaining why the more tightly coiled chains show less of the photophysical features of aggregation.

Self-Aggregation Versus Between-Chain Aggregation

Although we believe our understanding is clear as to how the choice of solvent affects the degree of aggregation for dilute conjugated polymer solutions, the relationship between solvent quality and degree of interchain interaction becomes murkier at higher polymer concentrations. Rothberg and coworkers (27, 47), Samuel and coworkers (48), and others (34, 35) have extensively studied the way in which interchain species form in conjugated polymer solutions as the choice of the solvent and temperature are varied. All these workers found an increase in the spectral signatures of interchain interaction in solvents less able to fully dissolve the conjugated polymer, leading to the suggestion that aggregation occurs primarily between chromophores on the same polymer chain. Although making polymer-solvent interactions less favorable does produce tighter coiling of the polymer chain (as illustrated in Figure 2), in "semi-dilute" polymer solutions, increasing polymer-polymer interactions relative to polymer-solvent interactions also leads to increased interpenetration of neighboring polymer strands (49). Thus,

we believe the increased number of interchain species formed in semi-dilute polymer solutions upon the addition of nonsolvents or upon lowering the temperature results from an increase in between-chain aggregation rather than from self-aggregation caused by coiling.

To test this view, we have performed a series of experiments (50, 51) on the conjugated polymer poly[2,5-bis(*N*-methyl-*N*-hexyl amino) phenylene vinylene] (BAMH-PPV) (52, 53), whose chemical structure is shown in the inset of Figure 3*a*. BAMH-PPV is a conjugated ionomer, a conjugated polymer functionalized with side groups that can be (controllably) electrically charged, in this case, by protonation with an organic acid. The electrostatic forces involved can dramatically change the conformation of an ionomer in solution as both the number of charges and polarity of the solvent are varied. For example, in nonpolar liquids that are good solvents for an uncharged ionomer, the polymer chains will collapse upon charging of a few percent of the side groups to minimize exposure of the charges and counterions to the surrounding solvent (54). This is illustrated for dilute solutions of BAMH-PPV in *o*-xylene in Figure 3*a*. The solid curve shows the DLS-determined coil size distribution for neutral BAMH-PPV, which, not surprisingly, is quite similar to that of MEH-PPV in CB (see Figure 2). The dashed curve shows that upon addition of enough camphor sulfonic acid (CSA) to protonate 7% of the amino side groups, the BAMH-PPV coil size shrinks by a factor of $\sim$3.

Figure 3*b* shows the effects of this charge-induced coil collapse on the electronic properties of the BAMH-PPV; the tight coiling of the polymer chain leads to an enormous blueshift of both the absorption and emission spectra (51). This blueshift, which is more dramatic than that observed in MEH-PPV solutions because of the larger change in coil radius (see Figure 1), is caused by the decrease in average conjugation length from the additional twisting of the backbone needed to fold the chain. Although the emission spectrum of the coiled BAMH-PPV does show a bit of a red tail (Figure 3*b*, thin dashed curve), which may be suggestive of a small degree of interchain contact, the fact that the overall spectral shift upon

Figure 3 Effect of protonation on chain conformation and electronic properties for a conjugated ionomer (51). (*a*) Size distributions (hydrodynamic radii) determined by DLS for dilute solutions of BAMH-PPV in *o*-xylene. The solid curve shows the results for a neutral solution, and the dashed curve shows the results for a solution with enough added camphor sulfonic acid (CSA) to protonate 7% of the amino side groups. The inset shows the chemical structure of BAMH-PPV. (*b*) Normalized UV-Visible absorption (*heavy curves*) and PL (*thin curves*) spectra for the same solutions of BAMH-PPV whose size distributions are shown in Part *a*. The solid curves show the results for the neutral solution, and the dashed curves show the result for the 7%-protonated solution. (*c*) Normalized (front-face collected) PL spectra for semi-dilute (1% w/v) solutions of neutral (*solid curve*) and 7%-protonated (*dashed curve*) solutions of BAMH-PPV in *o*-xylene. Absorption spectra are not shown because at this concentration the solutions have too high an optical density for accurate measurement.

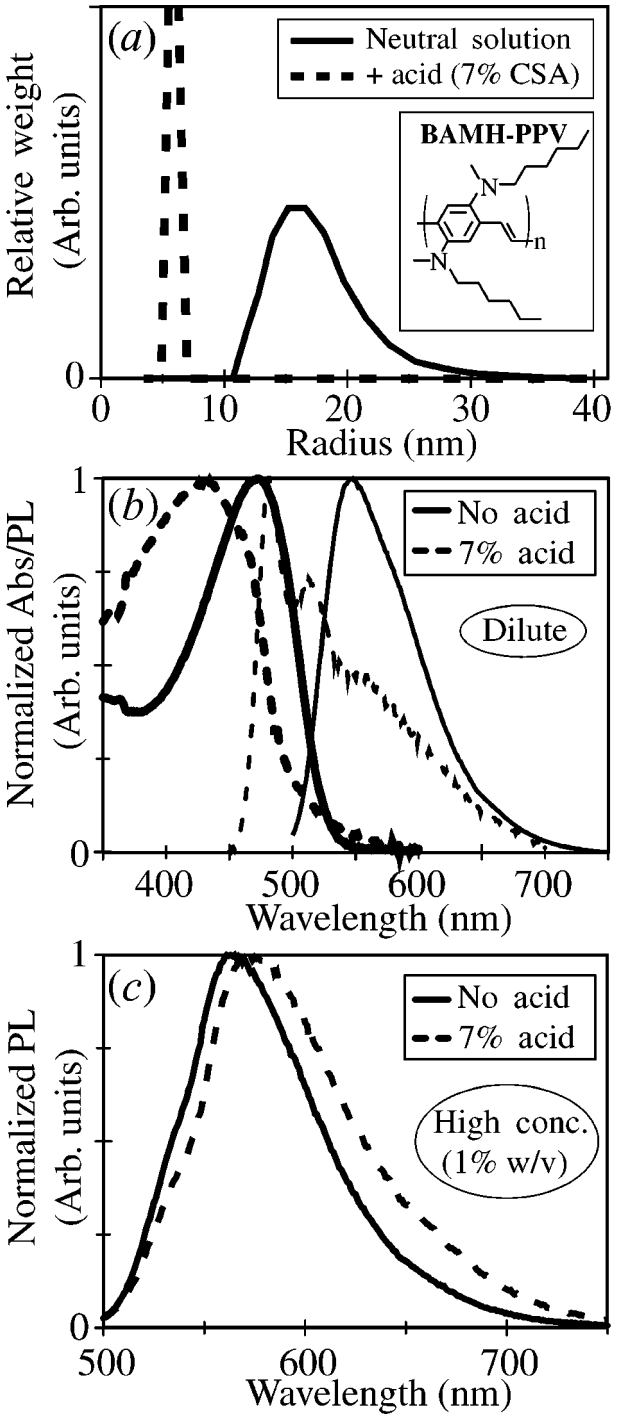
(a)
Neutral solution
+ acid (7% CSA)
BAMH-PPV
N
n
N
Relative weight
(Arb. units)
0
0
10
20
30
40
Radius (nm)
(b)
No acid
7% acid
Dilute
Normalized Abs/PL
(Arb. units)
1
0
400
500
600
700
Wavelength (nm)
(c)
No acid
7% acid
High conc.
(1% w/v)
Normalized PL
(Arb. units)
1
0
500
600
700
Wavelength (nm)

coiling is to the blue verifies that tightly coiled conjugated polymer chains in dilute solutions do not undergo a significant amount of self-aggregation. Figure 3*c* shows the PL spectra of semidilute (1% w/v) solutions of neutral (solid curve) and 7% CSA-protonated (dashed curve) BAMH-PPV. At this higher concentration, typical of what is used for spin-coating films, charging the amino side groups leads to a redshift of the emission. This is consistent with our picture that the electrostatically induced change in polymer-polymer and polymer-solvent forces not only alters the chain conformation but also increases interchain penetration, thus increasing the degree of chromophore aggregation (51).

Relationship Between Solution Aggregation and Film Morphology

Now that we have seen how the balance between polymer-polymer and polymer-solvent interactions affects the conformation and degree of interchain electrical contact in solution, the next question to address is how the morphology and degree of aggregation in conjugated polymer films are affected by the properties of the solutions from which they are cast. Both X-ray (55) and electron diffraction (56) studies indicate differences in the chain packing of MEH-PPV films cast from different solvents. In addition, Figure 4 shows scanning-force microscopy images of MEH-PPV films spin-cast under different conditions: from a 1% w/v solution in CB (top panel); from a 1% w/v solution in THF (center panel); and from solution followed by thermal annealing for several hours above the polymer's glass-transition temperature, T_g (lower panel) (57). The surface topography of each film is clearly different: The two as-cast films show the presence of topographic features ("bumps") that are a few-hundred nanometers in diameter and a few nanometers high, whereas the annealed film (note the color scale change in the figure) is smooth and homogeneous with very little surface roughness. Even though the images do not provide information about the conformation of individual chains in the films, the fact that each film has a recognizably distinct topography verifies that "memory" of the chain conformation in solution somehow persists through the spin-casting process, producing films with different underlying chain packing morphologies.

In a series of experiments, we have found that the number of bumps visible on the surface of as-cast MEH-PPV films increases as the polymer concentration in the solution from which the film was cast increases, and that the number of bumps tends to be higher in films cast from CB relative to films cast from THF at

Figure 4 5 μm $\times$ 5 μm scanning-force micrographs of MEH-PPV films cast under different conditions (57). (*Top panel*) MEH-PPV film cast from 1.0% w/v solution in CB. (*Center panel*) MEH-PPV film cast from 1.0% w/v solution in THF. (*Bottom panel*) MEH-PPV film cast from solution and then annealed for several hours above the glass transition temperature. The results are similar whether annealing is performed on CB-cast or THF-cast films. Note that the color scale representing the surface height is expanded in the bottom panel.

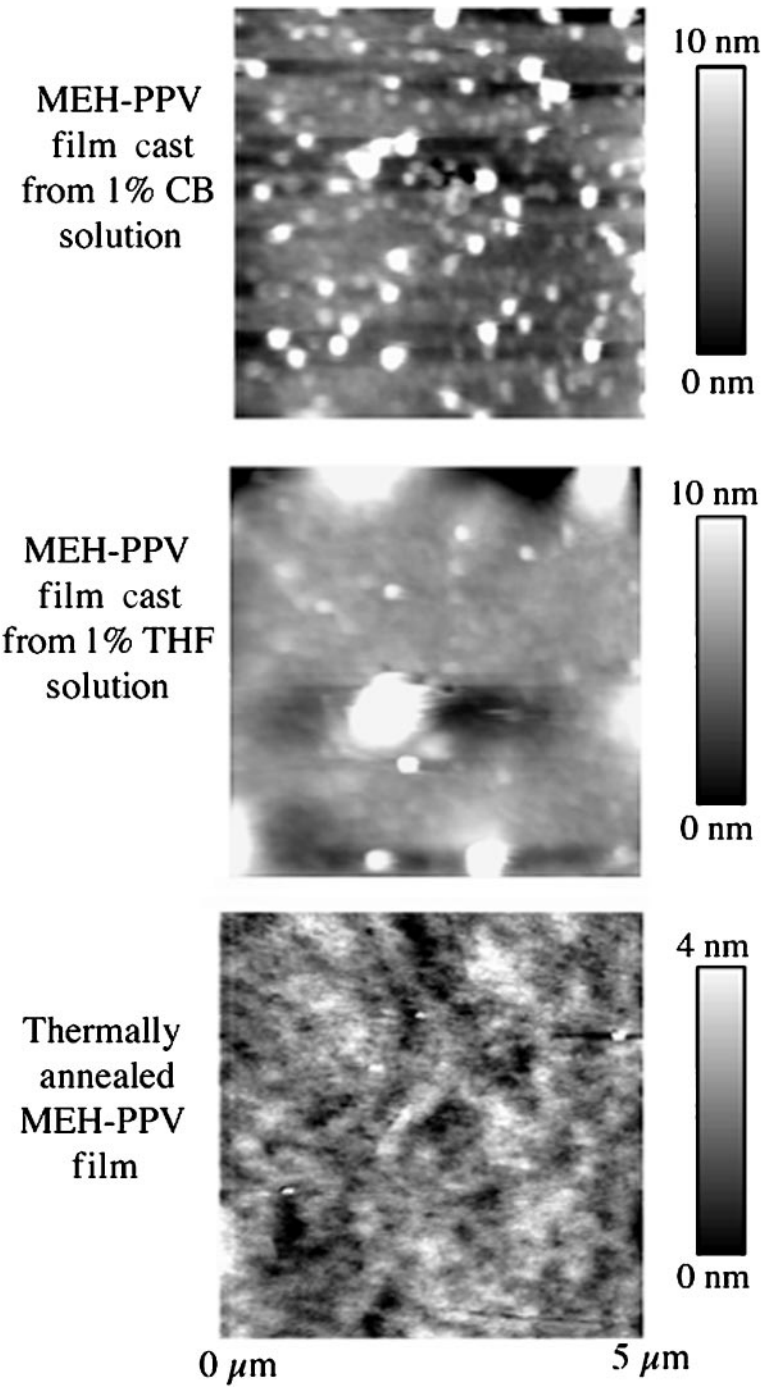
MEH-PPV film cast from 1% CB solution
10 nm
0 nm
MEH-PPV film cast from 1% THF solution
10 nm
0 nm
Thermally annealed MEH-PPV film
4 nm
0 nm
0 μm
5 μm

the same concentration (57). We have also seen that the number of bumps on the surface of as-cast BAMH-PPV films increases with both increasing solution polymer concentration and degree of protonation (at the high polymer concentrations needed for spin-casting) (51). This direct correlation between the degree of aggregation in solution and the presence of bumps on the corresponding films makes it quite tempting to assign the bumps to the existence of solution agglomerates, which contain a high fraction of aggregates, that survive the casting process and persevere in the film. We also note that the nearly featureless topography of the annealed MEH-PPV film in the lower panel of Figure 4 fits well with a picture in which heating above T_g allows the freely flowing chains in the polymer melt to untangle into lower-energy conformations. This presumed straightening of the polymer strands upon annealing would lead to better chain packing and thus a large increase in the degree of interchain interactions in annealed films relative to as-cast films.

THE RELATIONSHIP BETWEEN CHAIN PACKING AND THE PHOTOPHYSICS OF CONJUGATED POLYMER FILMS

Morphology Effects on the Steady-State Optical Properties of Conjugated Polymer Films

Now that it is clear that the processing history (e.g., the choice of solvent in the casting solution or thermal annealing) can lead to differences in film morphology, the next question to address is how these morphology differences affect the electronic properties of conjugated polymers. Single-molecule experiments by both Barbara and coworkers (58, 59) and Huser et al. (60, 61) have shown that changing the processing conditions can alter the emission properties of individual MEH-PPV chains. Similar processing-history-dependent variations in the PL of conjugated polymers also occur in bulk film samples; Figure 5*a* shows the PL spectra of

Figure 5 (*a*) Normalized PL spectra of the same MEH-PPV films whose scanning-force micrographs are presented in Figure 4. The heavy solid curve shows the PL from the THF-cast film, the dashed curve shows the PL from the CB-cast film, and the thin solid curve shows the PL from the annealed film. The overall PL quantum yield decreases in the order: THF-cast, CB-cast, annealed (57). (*b*) Spatially resolved photoluminescence (SRPL) spectra measured by collection-mode near-field scanning-optical microscopy (NSOM) from two different locations of an MEH-PPV film cast from a 1.0% w/v solution in CB. The solid curve shows the typical SRPL when the NSOM probed is positioned between the topographic features on the film's surface (compare *upper panel* of Figure 4), and the dashed curve shows the typical SRPL when the NSOM probe is positioned directly on top of one of the topographic features (68).

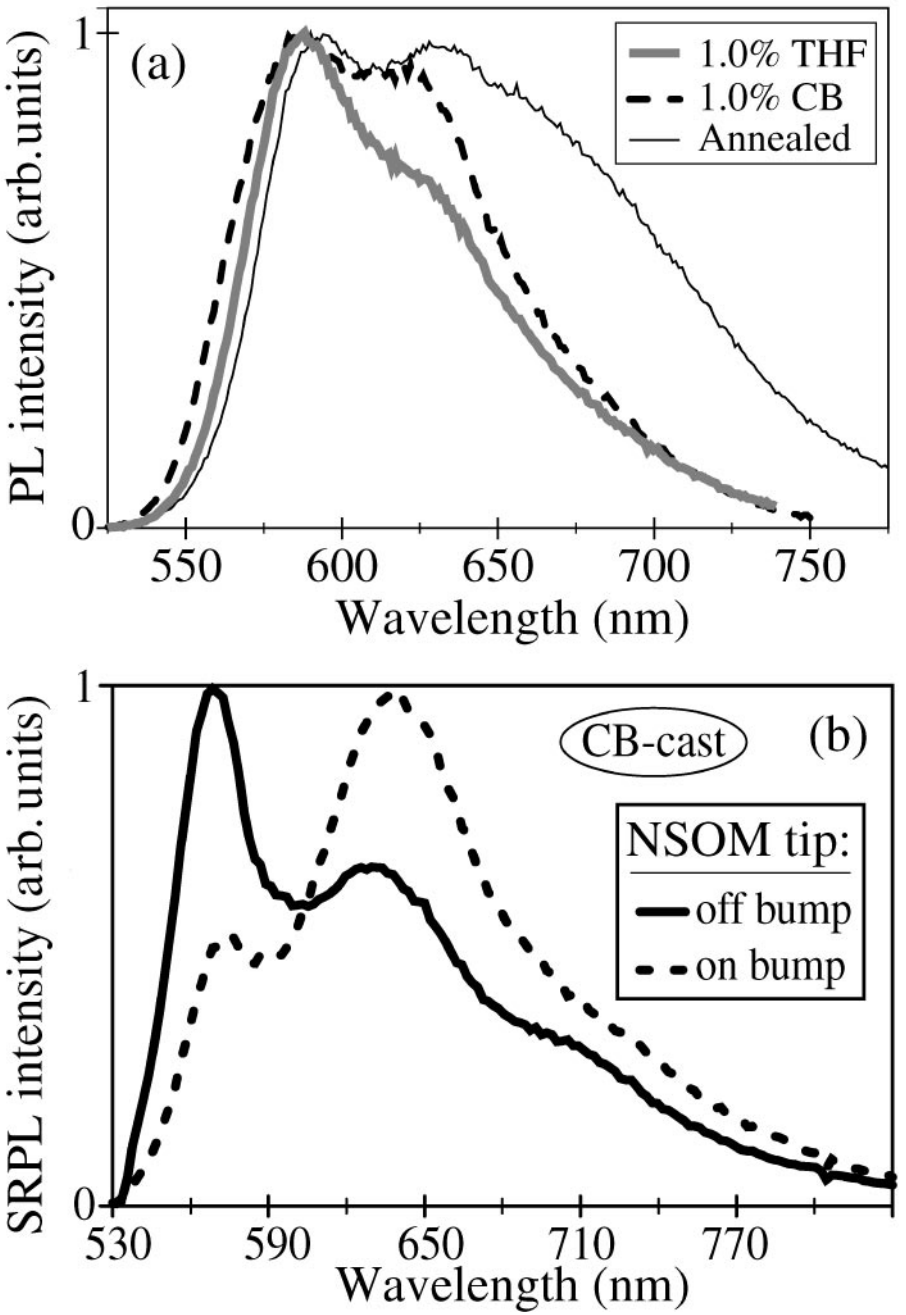
(a)
1.0% THF
1.0% CB
Annealed
PL intensity (arb.units)
1
0
550
600
650
700
750
Wavelength (nm)
(b)
CB-cast
NSOM tip:
off bump
on bump
SRPL intensity (arb.units)
1
0
530
590
650
710
770
Wavelength (nm)

the same three MEH-PPV films whose scanning-force micrographs are shown in Figure 4 (57). The figure makes it clear that as the degree of aggregation is increased by changing casting solvents from THF to CB or by annealing, the luminescence of the corresponding film both shows a change in vibronic coupling (Huang-Rhys parameter) and undergoes a noticeable shift to the red. Comparison to the work of Rothberg and coworkers (23, 27, 47) has led us to believe that the PL from annealed films is nearly entirely interchain. In addition to the redshift of the film PL, another sign of differing degrees of aggregation in films cast from different solvents is a significant change in emission quantum yield. Although not visible in Figure 5*a* because the spectra presented are normalized, the integrated emission intensity of the CB-cast film is much lower than that of the THF-cast film, and the emission quantum yield of the annealed film is even lower (57). All of this information is consistent with our picture that even basic electronic properties (such as the PL) of conjugated polymer films are largely determined by the presence of weakly emitting interchain species present in the solutions from which they were cast.

One way to assess whether the topographic bumps seen in Figure 4 really are associated directly with the spectral changes seen in Figure 5*a* is via near-field scanning-optical microscopy (NSOM) experiments (62). In the past few years, many groups have applied NSOM-based techniques to conjugated polymers and found that absorption and emission properties of conjugated polymer films are not spatially homogenous (63–67). The MEH-PPV films whose properties are shown in Figures 4 and 5*a* are no exception. Figure 5*b* compares a typical spatially resolved photoluminescence (SRPL) spectrum collected when the NSOM probe sits on top of one of the topographic bumps (dashed curve) to that collected when the NSOM tip is placed between the bumps (solid curve) (68). The SRPL spectrum associated with the bumps is almost always redshifted and has different vibronic coupling from the SRPL spectrum collected between the bumps, consistent with our assignment of the bumps to regions of the film associated with increased interchain interactions. In a series of NSOM photodegradation measurements, we also found that photo-oxidative quenching occurs more slowly for emission collected from on top of a bump than for emission collected between bumps (68). This is also consistent with the idea of more tightly packed chains in the bumps: The slower photodamage rate likely results from the increased difficulty for oxygen to diffuse into regions of the film where the chains are closely packed.

Morphology Effects on the Ultrafast Photophysics of Conjugated Polymer Films

In addition to the PL spectrum, changing the film morphology by changing the film processing conditions also affects other photophysical properties of conjugated polymers. Many groups have argued for the existence (or lack thereof) of interchain species in conjugated polymer films by comparing the emission dynamics of the PL to those of the excited-state absorption (19, 20, 43, 69–74). We performed a series of femtosecond pump-probe experiments on the MEH-PPV films whose properties

are shown in Figures 4 and 5 and found striking differences in the spectral dynamics as a function of film morphology (57). In particular, the agreement between the decay of the PL and that of the excited-state absorption depends sensitively on the chain morphology as well as the excitation intensity. We also found that both the interchain excited-state absorption and the effects of photo-oxidative damage have similar spectral signatures to that of the single-chain exciton (57). Given the similarity of the various possible excited-state spectral features and the fact that the film morphology determines both the degree of interchain contact and the susceptibility to photodamage, it is straightforward to reconcile many of the apparently contradictory results in the literature that came from groups studying samples processed in different ways (57).

Another example of literature results that have been affected by differences in film morphology comes in the behavior of conjugated polymer films at excitation densities high enough that excitons on neighboring chromophores can interact destructively, a phenomenon known as exciton-exciton annihilation (E-EA) (75). Several groups have measured the probability for E-EA (the so-called bimolecular recombination coefficient) in conjugated polymer films with results that vary by over an order of magnitude (71, 72, 75–77). We have made similar measurements on MEH-PPV films and determined that the probability for excitonic annihilation is roughly eight times higher in films cast from CB relative to films cast from THF (57). We also found that the probability for E-EA is higher in BAMH-PPV films cast from high-concentration protonated solutions than from neutral solutions (51). Both these results are consistent with the idea that E-EA depends on the overlap of two neighboring excitonic wave functions, which in turn depends on the relative positions of the adjacent conjugated polymer chromophores. The more tightly packed chains in CB-cast films of MEH-PPV (or protonated films of BAMH-PPV) allow for greater excitonic interaction than the more loosely packed chains in THF-cast films of MEH-PPV (or neutral films of BAMH-PPV), increasing probability for E-EA.

The fact that both the degree of E-EA and the nature of the excited-state absorption depend sensitively on film morphology also has important implications for the ability of conjugated polymers at high excitation densities to undergo spectral line-narrowing (78) or lasing (79). Several groups have noted that the line-narrowing phenomenon depends on the details of how the films were processed (78, 80, 81). We believe that this results from a competition between exciton depletion via stimulated emission gain (which is affected by any interchain excited-state absorption in the emission region) and excitonic annihilation (which, as just argued, also depends on the degree of interchain contact in the film) (57, 82). This suggests that adequate control over film morphology is one of the primary remaining obstacles to be overcome to achieve line-narrowing in electrically powered conjugated polymer devices. Overall, the results of experiments from many groups have shown that processing differences, such as heating the polymer solution during dissolution (50), growing the polymer films layer-by-layer using Langmuir-Blodgett (83, 84) or self-assembly techniques (85, 86),

altering the spin speed (87, 88), and thermal annealing (89–91), all can dramatically affect the optical properties and device performance of conjugated polymer films.

The Electronic Nature of Interchain Species in Conjugated Polymer Films

Despite all the evidence presented above that interchain species can and do form in conjugated polymer films, there is still relatively little known concerning the nature of the intermolecular excited state(s) and which of the various interchain species labels, if any, is most appropriate. One way to distinguish between the possible interchain species is to determine the degree of charge separation by measuring the dipole moment of the interchain excited state. Solvatochromism provides a powerful method for determining excited-state dipole moments by measuring the shift of the PL as the dielectric properties of the surrounding solvent are systematically changed (92). If the excited-state dipole moment is smaller than that of the ground state, as expected for neutrally delocalized excimers or aggregates, then increasing the polarity of the environment will stabilize the ground state more than the excited state, resulting in a blueshift of the emission. Conversely, if the excited-state dipole moment is larger than that of the ground state, as would be the case for charge-separated polaron pairs, then increasing the solvent polarity will stabilize the excited state more than the ground state, producing a redshifted emission. Thus, by studying how the interchain emission shifts in the presence of polar liquids, the interchain dipole moment, and hence the nature of the interchain species, can be revealed. Performing solvatochromic experiments on conjugated polymer films is not completely straightforward, however, because simple immersion of a film into a solvent only shifts the emission of the few chromophores near the film's surface, whereas the bulk of the emission is dominated by the much larger fraction of unsolvated chromophores residing in the film's interior. However, the solvatochromically shifted emission from the polymer/liquid interface can be captured selectively using NSOM, which has a shallow depth-of-field comparable to the diameter of the sub-wavelength tip (62).

The results of NSOM solvatochromism experiments on annealed MEH-PPV films (chosen because the emission from such films is almost entirely interchain; see Figure 5*a*) are shown in Figure 6 (93). For the majority of the annealed film's area ($\geq$95%), the application of polar liquids such as ethylene glycol (EG) or acetonitrile (MeCN) produces a blueshift of the interchain PL (Figure 6*a*). This blueshift with increasing liquid polarity indicates that the ground state of most chromophores in annealed MEH-PPV films possess a larger dipole moment than the emissive interchain excited state, typical of what is expected for an excimer or aggregate. In a few localized ($\sim$1-μm diameter) regions comprising less than 5% of the film's area, however, application of polar liquids produces a strong redshift of the interchain emission (Figure 6*b*) (93). This is what is expected

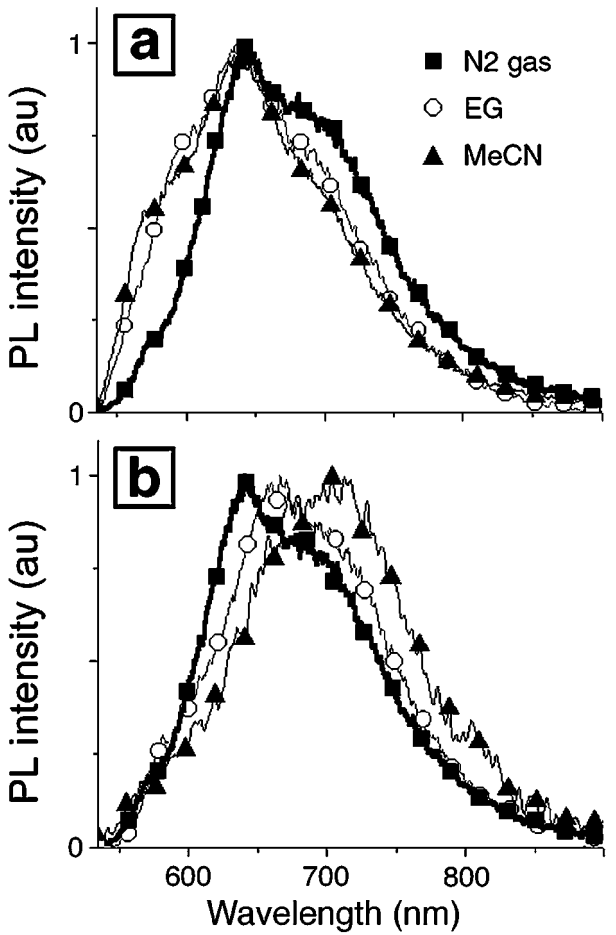

Figure 6 Solvatochromic behavior of the collection-mode SRPL spectra of an annealed MEH-PPV film when the film is immersed under different polar liquids: no solvent/N_2 gas (*heavy curves/solid squares*); ethylene glycol (EG, *thin curves/open circles*); acetonitrile (MeCN, *thin curves/solid triangles*). Panel *a* shows the results when the NSOM probe is placed over a region for which the SRPL blueshifts upon the application of polar liquids, as typical for over 95% of the film's area. Panel *b* shows the results when the NSOM probe is placed over one of the $\sim$1 μm spatially localized regions (which comprise $<$5% of the film's area) for which the SRPL redshifts upon the application of polar liquids. The spectra in both panels are shown on an absolute scale, verifying that the presence of polar liquids does not change the emission intensity. The SRPL spectra collected from the different locations with no solvent present on the film are indistinguishable (93).

for asymmetric interchain species such as exciplexes or polaron pairs. The variation in excited-state dipole moment observed in different locations throughout the film suggests the presence of an entire family of interchain species, each characterized by a different degree of charge separation. The fact that the large-dipole interchain species are found in spatially segregated domains implies that interchain charge separation is associated with the presence of defects such as cis-linkages or tetrahedral sites (94), chain ends (95), or carbonyl groups (96), which are likely to have phase segregated in the polymer melt during the annealing process. When the molecular weight of the polymer is lowered, the solvatochromically redshifting regions increase in spatial extent, suggesting that the defects that promote charge separation are intrinsic (93). We believe that excimers and/or aggregates are the dominant interchain species in conjugated polymer films, but that a whole variety of interchain species can form depending on the processing conditions and the nature of any intrinsic defects along the polymer backbone.

The Spatial Distribution of Interchain Species in Conjugated Polymer Films

Although NSOM solvatochromism strongly suggests that the majority of interchain species in conjugated polymer films are delocalized with little charge separation, this type of emission-based experiment cannot discern whether this delocalization takes place in both the ground and excited states (aggregates) or just in the excited state (excimers). Aggregates can be distinguished from excimers, however, using absorption-based spectroscopies to search for the presence of the redshifted ground-state aggregate band (24–26). Aggregates also can be distinguished by the fact that they are usually distributed inhomogeneously throughout a conjugated polymer film (63–67). As mentioned above, it is quite difficult to observe and spatially resolve the aggregate absorption band using transmission or PL-based excitation measurements because the oscillator strength of the transition is quite weak and the emission quantum yield is very low. These difficulties can be overcome by combining nonlinear absorption-based spectroscopies such as third harmonic generation (THG) with optical probe techniques such as NSOM (97). The low background associated with THG measurements allows for measurement of weak absorption signals, whereas the subwavelength spatial resolution of NSOM provides a means to measure the spatial distribution of any weakly absorbing aggregate species in the sample.

In THG-NSOM experiments on annealed MEH-PPV films, no contrast is observed as the NSOM tip is scanned across the sample when the third harmonic of the incident laser is resonant with the intrachain exciton absorption band, indicative of a uniform distribution of single-chain chromophores throughout the film (98). When the third harmonic of the incident laser frequency is tuned to the red of the main exciton absorption band (to 620 nm; see Figure 1), however, the THG-NSOM image shows many ~400-nm diameter, prolate-shaped domains

that comprise ∼20% of the film's area, as seen in Figure 7*a*. Similar THG-bright regions at $3\omega = 620$ nm are also seen (although much less frequently) in as-cast films, where they appear to be associated with the topographic bumps. Figure 7*b* shows that when the tip is placed over one of these bright regions, the THG spectrum shows a distinct absorption band that is redshifted from the main exciton absorption, suggestive of nanoscopic aggregation domains (98). Moreover, the bright features also have a distinct polarization, indicating that the polymer chains in these aggregation domains have a preferred orientational alignment. This polarization, in combination with the spatial distribution of the domains, suggests that they are likely formed in annealed films via a nucleation and growth mechanism, and in as-cast films from solution agglomerates that did not break up during spin-casting. Given their size and spatial frequency, these aggregation domains do not appear to be related to the solvatochromically redshifted domains discussed above: The solvatochromic experiments measure excited-state emission from the surface of the film (93), whereas the THG studies are sensitive to the nonlinear polarizability of the ground-state polymer chains throughout the entire bulk of the film (98). Thus, we believe the two NSOM measurements probe distinct, although coexisting, interchain species in annealed films of MEH-PPV.

UNDERSTANDING AND CONTROLLING ENERGY TRANSFER IN CONJUGATED POLYMERS

The Importance of Energy Transfer in Conjugated Polymers

One of the reasons that the presence of even small numbers of interchain species can have such a large effect on the electronic properties of conjugated polymer films is that energy transfer is facile in these materials. As mentioned earlier, the results of many experiments have established that energy migration via Förster transfer takes place rapidly, in just a few picoseconds (13–16). This allows excitations to flow efficiently to low-energy interchain states, where their emission can be quenched. For example, both McBranch and coworkers (99) and Bazan and coworkers (100) have observed "superquenching" of conjugated polymers in solution upon the addition of electron-accepting quenchers and surfactants. In these experiments, the polymer is a PPV derivative with negatively charged side groups and the quencher is positively charged. The addition of quencher and surfactant changes the conformation of the polymer (in much the same manner as the protonation of BAMH-PPV; see Figure 3), bringing many chromophores within a Förster radius (the distance at which the probability for Förster energy transfer is 50%) of the quencher. Thus, the excitations on many segments have an easy pathway to migrate to the site in contact with the quencher, allowing a single quencher molecule to extinguish the emission from hundreds of chromophores (99, 100). Experiments on single conjugated polymer molecules also show evidence that the emission from tightly coiled chains comes from a single chromophore, supporting the conclusion


(a)

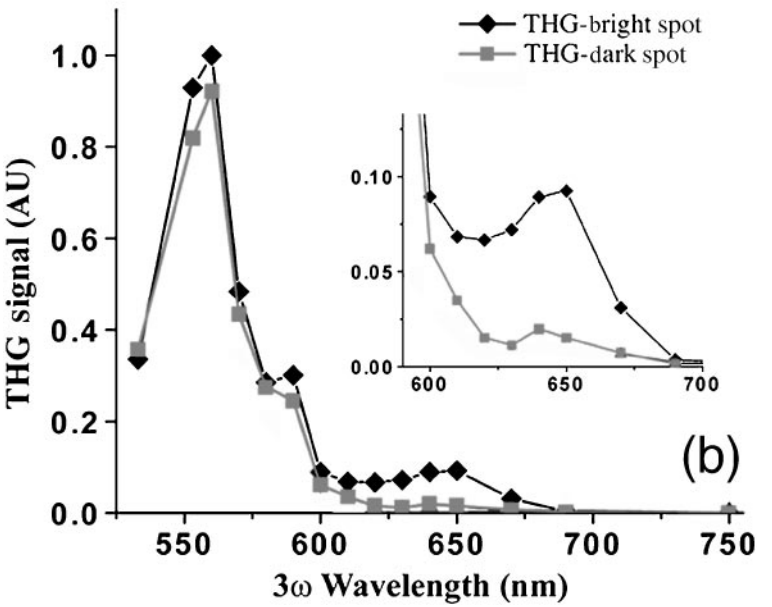
THG-bright spot
THG-dark spot
THG signal (AU)
1.0
0.8
0.6
0.4
0.2
0.0
550
600
650
700
750
3ω Wavelength (nm)
0.10
0.05
0.00
600
650
700
(b)

that a single low-energy site can quantitatively "harvest" the excitations from all the nearby conjugated segments (58–61).

None of the above experiments, however, address the fundamental questions of how easily energy migrates along the backbone of a conjugated polymer chain rather than through space between conjugated segments, or how this energy flow can be controlled or directed. We have shown that the use of a host/guest composite material both facilitates control over energy flow in conjugated polymers and allows the roles of intrachain and interchain energy transfer to be cleanly separated (101–103). The composite material was synthesized starting with a nanoporous silica glass (MCM-41) that was aligned in a magnetic field via a silica-surfactant liquid-crystalline intermediate (104). After condensation and calcination of the silica host, the resulting mesoporous glass is surface-treated with organic groups to promote compatibility of the hexagonally arrayed $\sim$22 Å-diameter channel interiors with the MEH-PPV guest, which is incorporated from solution (105). Polarized spectroscopy experiments indicate that in the final composite material, the majority of the MEH-PPV chain segments are oriented and isolated from each other by incorporation into the aligned channels of the porous glass (101–103, 105, 106). A small amount of unincorporated polymer also resides outside the channels in the composite, with randomly oriented chromophores that may form interchain contacts; a schematic picture of the composite is given in the inset to Figure 8*b*. It is this complexity, the presence of two distinct types of polymer environments in a single material, that allows for the control over energy transfer and provides a means to distinguish inter- and intrachain energy transport (101, 102).

Intrachain versus Interchain Energy Transfer in Conjugated Polymers

Figure 8*a* shows the results of steady-state PL measurements on the composite material with the pores oriented vertically in the lab frame and the excitation light polarized horizontally, perpendicular to the pores (101–103). In MEH-PPV films excited with polarized light, the emission is nearly completely depolarized, indicating that energy transfer scrambles the direction of the excitations' transition

←

Figure 7 (*a*) Collection-mode THG-NSOM image of an annealed MEH-PPV film with the incident laser tuned to 1.86 μm ($3\omega = 620$ nm). The observed contrast has no relation to the film topography (which is featureless; see *lower panel*, Figure 4) and is discernable only at 3ω wavelengths between 620 and 670 nm. (*b*) Spectrally resolved THG-NSOM spectra collected from different regions of an annealed MEH-PPV film. The diamonds/dark curve show the THG spectrum collected with the NSOM probe positioned above one of the bright regions in Panel *a*, while the squares/lighter curve show the THG spectrum collected when the NSOM probe is positioned over one of the dark regions in Panel *a*. The THG-dark spectrum matches well with the linear absorption spectrum of the annealed film (98).

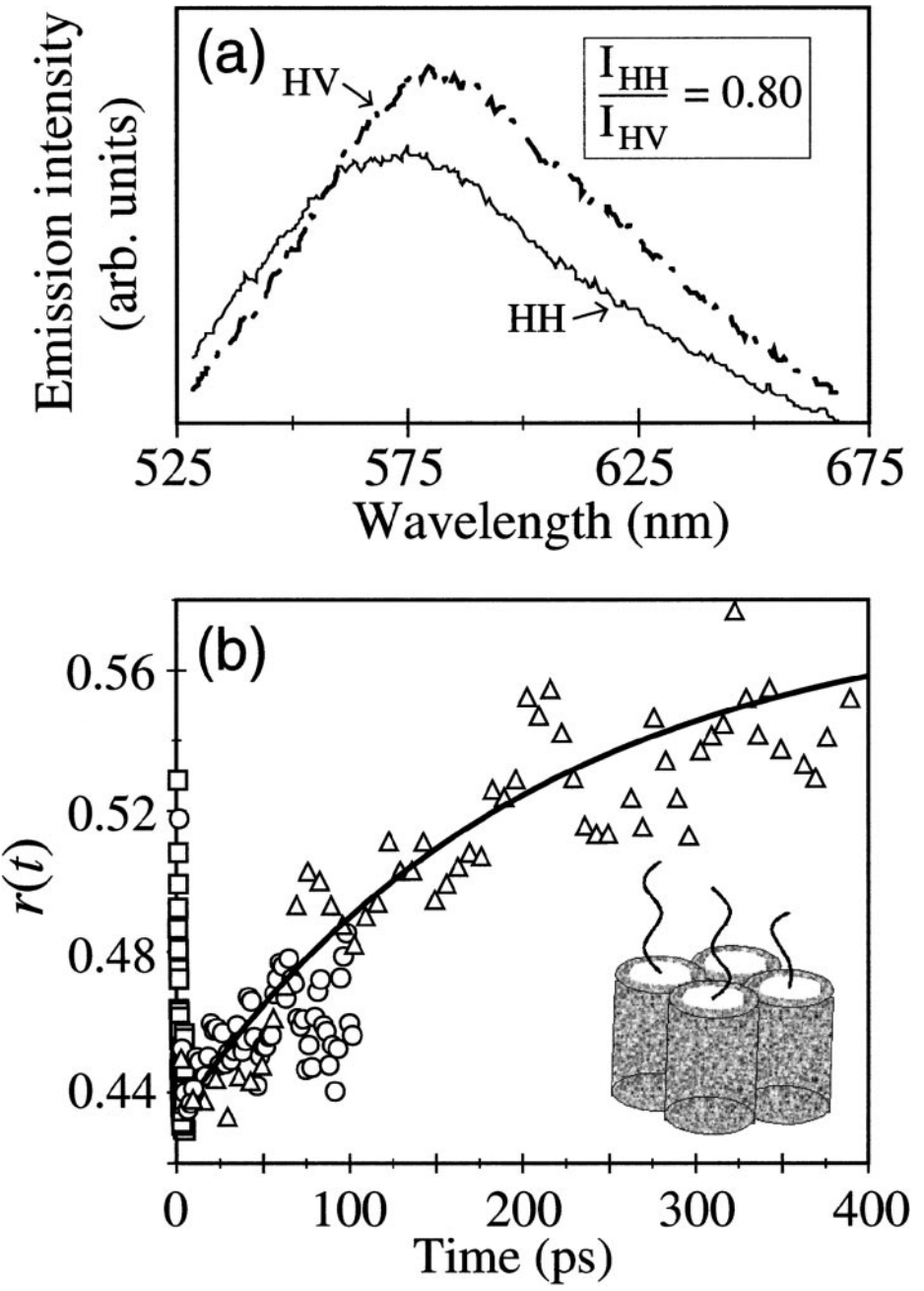
(a)
HV
HH
$\frac{I_{HH}}{I_{HV}} = 0.80$
Emission intensity
(arb. units)
525
575
625
675
Wavelength (nm)
(b)
0.56
0.52
0.48
0.44
r(t)
0
100
200
300
400
Time (ps)

dipoles on a rapid timescale compared with the emission lifetime (103). In the composite, however, more light is emitted polarized in the direction along the pores (HV) than along the direction of the excitation polarization (HH). This suggests that excitations on the short, randomly oriented segments outside the pores, which are preferentially excited by the light polarized against the pore direction, migrate to the longer segments that are rigidly held in the pores. The driving force for this energy migration can be seen in the redshift of the HV emission relative to the HH emission in Figure 8*a*: There is a clear gradient for moving energy from the coiled and nonaligned polymer segments outside the channels to the straight and aligned segments trapped within the pores.

Figure 8*b* shows the results of time-resolved polarized luminescence experiments on the composite material (101–103). Immediately aftert excitation, all of the emission comes from the chromophores that were originally excited, leading to a high value of the anisotropy, $r(t)$. As energy migrates between segments, memory of this initial polarization is lost, leading to a decay of the anisotropy in the first few picoseconds following excitation. Following this initial decay, Figure 8*b* shows the remarkable result that the emission polarization spontaneously increases with time. As with the steady-state data in Figure 8*a*, the only way to explain this increase in anisotropy is if energy initially deposited on randomly oriented polymer segments exterior to the pores is driven to the aligned segments in the interior, leading to a net increase in emission polarization. Thus, the composite material behaves in many ways as an artificial photosynthetic reaction center: The randomly oriented, short-conjugation antenna chromophores outside the channels harvest light with all polarizations, followed by unidirectional energy migration to the aligned, lower-energy chromophores in the channel interiors. Moreover, energy in the composite material is transported with very little loss: The polymer segments in the interior are no farther downhill in energy than the longest segments typically present in a conjugated polymer film (101, 102).

←

Figure 8 (*a*) Steady-state PL spectra from MEH-PPV/mesoporous silica composites. The channels of the composite are oriented vertically in the lab frame. When exciting with horizontally polarized light, the solid curve shows the horizontally polarized PL spectrum (HH) and the dashed curve shows the vertically polarized PL spectrum (HV). The spectra are plotted on an absolute intensity scale, making it clear that more light is emitted along the pore axis than along the direction of the excitation polarization. (*b*) Time-resolved 590-nm emission anisotropy of MEH-PPV/mesoporous silica composites following excitation polarized parallel to the pores. The anisotropy, which measures only the polarization memory of the emitted light and is not affected by the emission lifetime, is defined by $r(t) = [||(t) - \perp(t)]/[||(t) + 2\perp(t)]$, where $||(t)$ is the intensity of the light emitted parallel to the excitation polarization and $\perp(t)$ is the intensity of the light emitted perpendicular to the excitation polarization. The different symbols represent scans taken with different time spacings between points. The inset shows a schematic diagram of the structure of the composite material (101).

The anisotropy rise seen in Figure 8*b* also allows us to make arguments about the relative efficiency of inter- and intrachain energy transport in conjugated polymers (101–103). The composite material has enough room physically for only one MEH-PPV chain per pore. Thus, energy migration from chromophores outside the pores to chromophores inside the pores must take place along the polymer backbone. Figure 8*b* shows that the time for the anisotropy rise, which results from energy flowing into the pores along the backbone, is roughly two orders of magnitude longer than the initial rapid anisotropy loss caused by through-space energy transport via Förster transfer. This observation that interchain energy transport is more rapid than intrachain transport is also consistent with work studying exciton trapping in poly(fluorene)-based copolymers (107). We believe that intrachain energy migration along the polymer backbone requires physical reorientation of the polymer segments ("ironing out the kinks") to facilitate communication between regions of broken conjugation (101–103). Thus, intrachain energy transfer is slow because the necessary motions take time and are likely to be thermally activated. Interchain energy transfer (and here we use "interchain" to include through-space interactions between different chromophores along the same polymer backbone) requires nothing more than physical proximity of polymer segments that are strongly dipole-dipole coupled.

IMPLICATIONS FOR CONJUGATED POLYMER-BASED OPTOELECTRONIC DEVICES

The Role of Film Morphology in Device Performance

The fact that between-chain energy transfer is facile, in combination with our observations that the morphology and degree of interchain interactions vary with casting conditions, has important implications for the performance of optoelectronic devices based on conjugated polymers. Figure 9 compares the behavior of ITO/MEH-PPV/Ca:Al sandwich structure LEDs where the active MEH-PPV layers were spin-cast from either a CB solution or a THF solution, the same processing conditions explored in Figures 4–7 (57). Figure 9*a* demonstrates that the THF-cast devices have a higher turn-on voltage and lower working current than their CB-cast counterparts. As argued above, the more open and straight polymer chains in CB-cast films form a larger number of interchain contacts, facilitating

Figure 9 Performance characteristics of ITO/MEH-PPV/Ca:Al sandwich structure LEDs based on 120-nm thick MEH-PPV films spin-cast from different solvents. (*a*) Typical current versus voltage curves, for LEDs based on 1.0% w/v CB-cast MEH-PPV films (*diamonds*) and 1.0% w/v THF-cast films (*open circles/thin solid curve*). (*b*) EL quantum efficiencies for the same LEDs whose I-V curves are shown in Panel *a*. LED based on 1.0% w/v CB-cast film (*dashed curve*), and LED based on 1.0% w/v THF-cast film (*solid curve*) (57, 89).

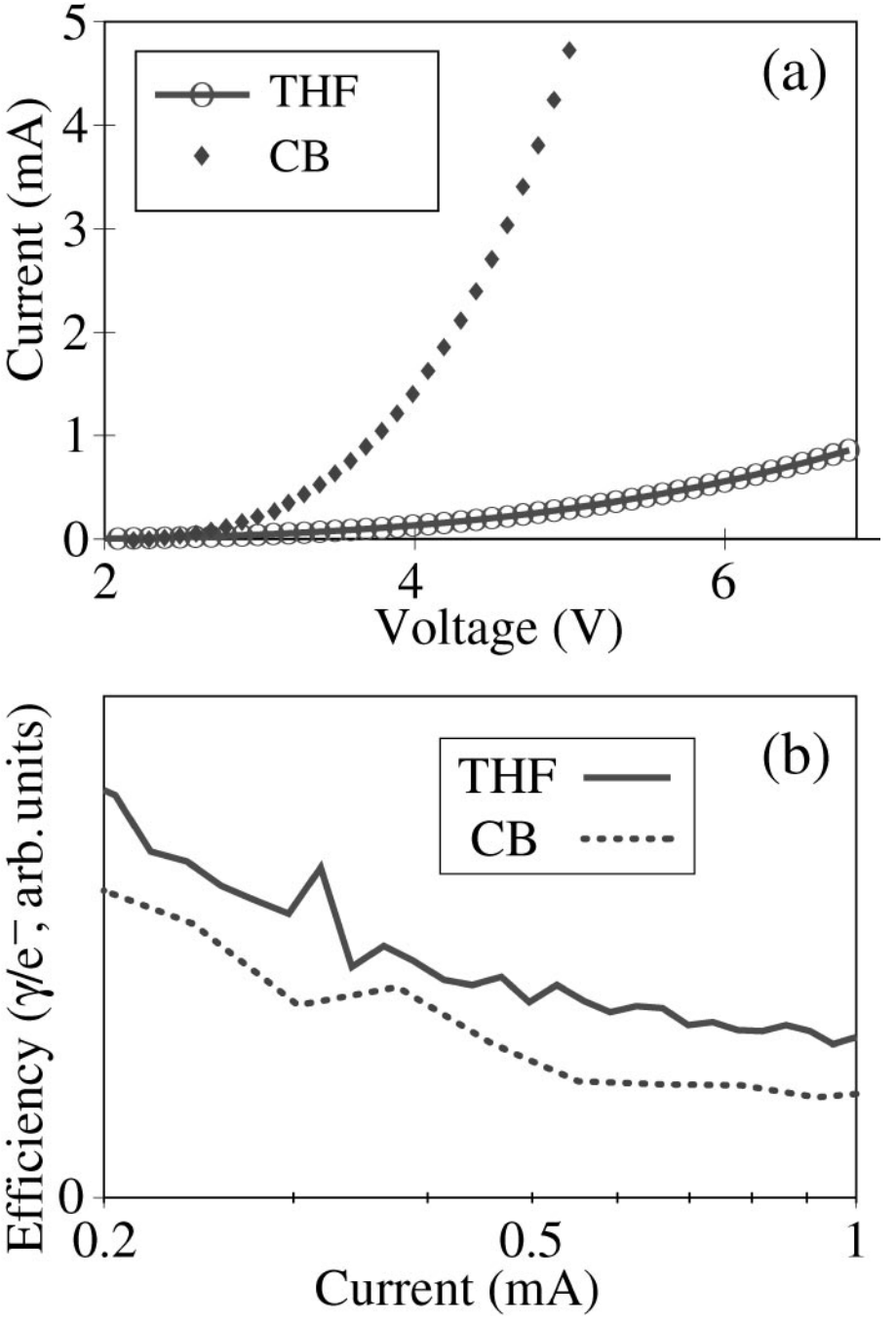
(a)
THF
CB
Current (mA)
Voltage (V)
0
1
2
3
4
5
2
4
6
(b)
THF
CB
Efficiency (γ/e⁻, arb. units)
Current (mA)
0
0.2
0.5
1

charge transport between chains and thus allowing higher operating currents in the device. THF-cast films, in contrast, form fewer interchain contacts, making it difficult for carriers to migrate through the film; if the carriers have low mobility, they will not easily be able to leave the region near the electrodes, leading to "space-charge limited injection" (108).

The fact that the current that can be injected into a conjugated polymer film varies with morphology illustrates a fundamental trade-off in optimizing the properties of conjugated polymer-based LEDs. Once the injected carriers recombine and an exciton is formed, the highest luminescence efficiency results from films with the least amount of interchain interactions because even a single interchain species can quench the emission of hundreds of nearby excitons. To form emissive excitons by electrical injection, however, higher carrier densities and mobilities are required, necessitating a high degree of interchain contact in the device. This trade-off is demonstrated in Figure 9*b*, which shows the relative EL quantum efficiencies (photons/electron) of the same LED's whose current-voltage curves are shown in Figure 9*a* (57). Despite the much lower working current and brightness, the EL efficiency of the device based on the THF-cast film is higher than that of the CB-cast film, suggesting that the few injected carriers that do manage to recombine in the center of the film create single-chain excitons without significant quenching by nearby interchain states. Many more carriers flow through the bright devices based on CB-cast films, but a significant fraction of those that recombine do so where the energy can be rapidly transferred to weakly luminescent interchain sites, reducing the EL efficiency. Several groups have observed a similar trade-off when attempting to alter interchain contact by using materials with bulky (109) or dendritic (110) side groups, resulting in higher EL efficiencies but lower working currents as the separation between chromophores is increased.

Despite this trade-off, it is possible to choose the morphology of a conjugated polymer film to optimize the performance of light-emitting devices. For example, we have fabricated heterostructure devices consisting of layers of MEH-PPV cast from CB sandwiched around a central layer of MEH-PPV cast from THF (89). The idea is to have high-mobility layers near the electrodes to facilitate charge injection, and a low-mobility layer in the center to promote recombination with higher luminescence efficiency. The tri-layer device works well, and has an EL efficiency that is more than double that of comparable devices based on only a single cast layer. In addition to improving charge injection by layering, the high degree of interchain contact produced by annealing also provides a mechanism to improve charge transport relative to as-cast films (89). Despite the lower PL quantum efficiency of annealed films, devices based on annealed films surprisingly can have higher EL efficiencies than those based on as-cast films. We believe that the smoothing of the surface of conjugated polymer films that takes place on annealing (see Figure 4) leads to better interfacial contact at the cathode, which in combination with the improved mobility results in a more balanced injection of electrons and holes that more than compensates for the

interchain losses in luminescence efficiency. Lee, Park, and coworkers have carried this idea of annealing conjugated polymer films one step further by annealing an entire MEH-PPV LED after the top electrode has been evaporated into place, and found even further enhancement of both the working current and the EL efficiency (90, 91).

SUMMARY AND THE FUTURE OF CONJUGATED POLYMER-BASED DEVICES

Throughout this paper, we have argued that a variety of interchain species can exist in conjugated polymer films and that both the degree to which they form and their chemical nature depend sensitively on the way in which the film was prepared. Conjugated polymer chains in solution can take on different physical conformations and are subject to different degrees of interchromophore contact as the polymer-polymer and polymer-solvent interactions are varied through the choice of solvent and polymer concentration. Memory of the solution coil shape and degree of aggregation is carried through the spin-coating process and endures into the film; thermal annealing also can alter the degree of interchain contact in the film. Films with higher average degrees of interchain contact have lower luminescence quantum yields, higher probabilities for excitonic annihilation, lower rates of photo-oxidative damage, and higher carrier mobilities than films with a lesser degree of interchain interactions. The fact that interchain energy transfer is more facile than energy migration along the backbone implies that the energy of emissive excitons can be easily harvested by only a few weakly emissive interchain species, magnifying their impact on device performance. The role of interchain species in conjugated polymers has been controversial because different groups studied materials processed under different conditions with different underlying morphologies, making it no surprise that so many authors have reached diverse conclusions. The main conclusion of this work is that the electronic behavior of conjugated polymers cannot be described simply as a "plastic free electron gas"; the molecular nature of these materials is critical to understanding their optical and electrical properties.

Many groups are working hard at improving the efficiency of polymer-based devices by altering the device architecture (e.g., by addition of electron- or hole-transport layers or addition of LiF tunnel barriers at the electrodes). In the results described above, however, the architecture of the devices was held constant and only the morphology of the film was varied to alter device performance. Thus, the methods for controlling morphology mentioned here (changing solvents or polymer concentration, thermal annealing, casting multiple polymer layers from different solvents, etc.) can be used in combination with more traditional engineering approaches to improve the efficiency of light-emitting polymer-based devices. Film morphology also plays a potential role in the degradation of polymer-based optoelectronic devices. The fact that polymer films are spatially inhomogeneous

suggests that current injection will take place preferentially at just a few sites on the film's surface. This means that most of the current in the device will flow through those pathways with the highest carrier mobilities, that is, those where the interchain coupling is the strongest. If the current density through these paths is large, the polymer around them will be heated and likely anneal, causing the regions to grow in size and have decreased luminescence: Such regions are possibly the source of the "black spots" observed prior to device failure. It is also becoming increasingly clear that changes in morphology during device operation are responsible for both the lower EL efficiency and the need for increased drive voltage to maintain brightness during device aging (111).

We believe that future improvements in device performance will center on new ways for tailoring the chain conformation and degree of interchain interactions for particular applications: For example, maximum chain overlap would be optimal for photovoltaic devices that require high charge transport and minimal luminescence efficiency, although the trade-off between high mobilities and good luminescence efficiency is more subtle for LEDs. We feel that the first steps toward having the necessary degree of control over morphology come from working with materials like the conjugated ionomers described above. By taking advantage of electrostatic forces, it should be possible to finely tune the polymer chain packing as well as to produce films with a graded morphology that varies continuously from the electrodes to the central recombination zone. Finally, the use of polymer-based composite materials offers an entirely new method for controlling chain conformation and thus device performance. A device based on conjugated polymer chains encapsulated in mesoporous silica would have the advantage of high carrier mobilities because all the charge conduction would be along individual chains: No interchain hopping events would be required. The recombination yield for electrons and holes injected onto a single chain should be unity, and there should be no weakly emissive interchain states to quench the luminescence of the excitons that form on single polymer chains. Clearly, with adequate control over morphology, there is an enormous potential waiting to be tapped for the use of conjugated polymer in numerous optoelectronic applications.

ACKNOWLEDGMENTS

This work was supported by the National Science Foundation under grant DMR-9971842, and the Petroleum Research Fund of the American Chemical Society under grants 32773-G6 and 37029-AC5,7. B.J.S. is a Cottrell Scholar of Research Corporation, an Alfred P. Sloan Foundation Research Fellow, and a Camille Dreyfus Teacher-Scholar. B.J.S gratefully thanks all the coauthors who made this work possible, including Thuc-Quyen Nguyen, Ignacio B. Martini, Richard D. Schaller, Richard J. Saykally, Ilan Benjamin, Mark E. Thompson, Junjun Wu, and Sarah H. Tolbert. We also thank Geoff Lindsay and John Stenger-Smith for supplying the BAMH-PPV samples used in this work.

The *Annual Review of Physical Chemistry* is online at http://physchem.annualreviews.org

LITERATURE CITED

1. Friend RH, Gymer RW, Holmes AB, Burroughes JH, Marks RN, et al. 1999. *Nature* 397:121–28
2. Kraft A, Gramisdale AC, Holmes AB. 1998. *Chem. Int. Ed. Engl.* 37:402–28
3. Braun D, Heeger AJ. 1991. *Appl. Phys. Lett.* 58:1982–84
4. Gustafsson G, Cao Y, Treacy GM, Flavetter F, Colinari N, Heeger AJ. 1992. *Nature* 357:477–79
5. Burroughes JH, Bradley DDC, Brown AR, Marks RN, Mackay K, et al. 1990. *Nature* 347:539–41
6. Brabec CJ, Sariciftci NS, Hummelen JC. 2001. *Adv. Funct. Mater.* 11:15–26
7. Huitema HEA, Gelinck, GH, van der Putten PH, Kuijk KE, Hart CM, et al. 2001. *Nature* 414:599
8. Su W-P, Schrieffer JR, Heeger AJ. 1979. *Phys. Rev. Lett.* 42:1698–701
9. Holzer W, Penzkofer A, Gong S-H, Bradley DDC, Long X, Bleyer A. 1997. *Chem. Phys.* 224:315–26
10. Brédas J-L, Cornil D, Beljonne D, dos Santos DA, Shuai Z. 1999. *Acct. Chem. Res.* 32:267–76
11. Brédas J-L, Street GB. 1985. *Acct. Chem. Res.* 18:309–15
12. Scholes DG, Larsen DS, Fleming GR, Rumbles G, Burn PL. 2000. *Phys. Rev. B* 61:13670–78
13. Kersting R, Lemmer U, Mahrt RF, Leo K, Kurz H, et al. 1993. *Phys. Rev. Lett.* 70:3820–23
14. Kersting R, Mollay B, Rusch M, Wenisch J, Leising G, Kaufmann HF. 1997. *J. Chem. Phys.* 106:2850–64
15. Lemmer U, Mahrt RF, Wada Y, Greiner A, Bässler H, Göbel EO. 1993. *Chem. Phys. Lett.* 209:243–46
16. Hayes GR, Samuel IDW, Phillips RT. 1995. *Phys. Rev. B* 52:11569–72
17. Graupner W, Leising G, Lanzani G, Nisoli M, DeSilvestri S, Scherf U. 1995. *Chem. Phys. Lett.* 246:95–100
18. Blatchford JW, Jessen SE, Lin BL, Lih JJ, Gustafson TL, et al. 1996. *Phys. Rev. Lett.* 76:1513–16
19. Yan M, Rothberg LJ, Kwock EW, Miller TM. 1995. *Phys. Rev. Lett.* 75:1992–95
20. Schwartz BJ, Hide F, Andersson M, Heeger AJ. 1997. *Chem. Phys. Lett.* 265: 327–33
21. Jenekhe SA, Osaheni JA. 1994. *Science* 265:765–68
22. Samuel IDW, Rumbles G, Collison CJ. 1995. *Phys. Rev. B* 52:R11753–56
23. Jakubiak R, Collison CJ, Wan WC, Rothberg LJ, Hsieh BR. 1999. *J. Phys. Chem. A* 103:2394–98
24. Lemmer U, Heun S, Mahrt RF, Scherf U, Hopmeier M, et al. 1995. *Chem. Phys. Lett.* 240:373–78
25. Blatchford JW, Jessen SW, Lin L-B, Gustafson TL, Fu D-K, et al. 1996. *Phys. Rev. B* 54:9180–89
26. Gelinck GH, Staring EGJ, Hwang DH, Spencer GCW, Warman JM. 1997. *Synth. Met.* 84:595–96
27. Collison CJ, Rothberg LJ, Treemaneekarn V, Li Y. 2001. *Macromol.* 34:2346–52
28. Gelinck GH, Warman JM, Staring EGJ. 1996. *J. Phys. Chem.* 100:5485–91
29. Yan M, Rothberg LJ, Papadimitrakopoulos F, Galvin ME, Miller TM. 1994. *Phys. Rev. Lett.* 72:1104–7
30. Gebler DD, Wang YZ, Fu DK, Swager M, Epstein AJ. 1998. *J. Chem. Phys.* 108: 7842–48
31. Conwell EM. 1998. *Phys. Rev. B* 57: 14200–2
32. Greenham NC, Samuel IDW, Hayes GR, Phillips RT, Kessener YARR, et al. 1995. *Chem. Phys. Lett.* 241:89–96

33. Zheng M, Bai GL, Zhu D. 1998. *J. Photochem. Photobiol. A* 116:143–45
34. Hsu J-H, Fann WS, Tsao P-H, Chuang K-R, Chen S-A. 1999. *J. Phys. Chem.* 103: 2375–80
35. Chang R, Hsu J-H, Fann WS, Yu J, Lin SH, et al. 2000. *Chem. Phys. Lett.* 317:153–58
36. Hoofman RJOM, deHaas MP, Siebbeles LDA, Warman JM. 1998. *Nature* 392:54–56
37. McBranch D, Campbell IH, Smith DL, Ferraris JP. 1995. *Appl. Phys. Lett.* 66: 1175–77
38. Bradley DDC. 1993. *Synth. Met.* 54:401–15
39. Kobrak MN, Bittner ER. 2000. *Phys. Rev. B* 62:11473–86
40. Wohlgenannt M, Tandon K, Mazumdar S, Ramasesha S, Vardeny ZV. 2001. *Nature* 409:494–97
41. Cao Y, Parker I, Yu G, Zhang C, Heeger AJ. 1999. *Nature* 397:414–17
42. Wilson JS, Dhoot AS, Seeley AJA, Khan MS, Friend RH. 2001. *Nature* 413: 828–31
43. Rothberg LJ, Yan M, Papadimitrakopoulos F, Galvin ME, Kwock EW, Miller TM. 1996. *Synth. Met.* 80:41–58
44. Nguyen T-Q, Doan V, Schwartz BJ. 1999. *J. Chem. Phys.* 110:4068–78
45. Wang SJ, Bazan GC, Tretiak S, Mukamel S. 2000. *J. Am. Chem. Soc.* 122:1289–97
46. Cornil J, dos Santos DA, Crispin X, Silbey R, Brédas J-L. 1998. *J. Am. Chem. Soc.* 120:1289–99
47. Wang P, Collison CJ, Rothberg LJ. 2001. *J. Photochem. Photobiol. A* 144:63–68
48. Samuel IDW, Rumbles G, Collison CJ, Moratti SC, Holmes AB. 1998. *Chem. Phys.* 227:75–82
49. Melinchenko YuB, Wignall GD. 1997. *Phys. Rev. Lett.* 78:686–89
50. Nguyen T-Q, Yee RY, Schwartz BJ. 2001. *J. Photochem. Photobiol. A* 144:21–30
51. Nguyen T-Q, Schwartz BJ. 2002. *J. Chem. Phys.* 116:8198–208
52. Stenger-Smith JD, Zarras P, Merwin LH, Shaheen SE, Kippelen B, Peyghambarian N. 1998. *Macromolecules* 31:7566–69
53. Stenger-Smith JD, Norris WP, Chafin AP, Sackenger ST. 1998. *U.S. Patent 5,604, 292*
54. Lantman CW, Macknight WJ, Lundberg RD. 1989. *Annu. Rev. Mater. Sci.* 19:295–317
55. Yang CY, Hide M, Díaz-García MA, Heeger AJ, Cao Y. 1998. *Polymer* 39: 2299–304
56. Weir BA, Marseglia EA, Chang SM, Holmes AB. 1999. *Synth. Met.* 101:154–55
57. Nguyen T-Q, Martini IB, Liu J, Schwartz BJ. 2000. *J. Phys. Chem. B* 104:237–55
58. Hu DH, Yu J, Barbara PF. 1999. *J. Am. Chem. Soc.* 121:6936–37
59. Yu J, Hu DH, Barbra PF. 2000. *Science* 289:1327–30
60. Huser T, Yan M. 2001. *J. Photochem. Photobiol. A* 144:43–51
61. Huser T, Yan M, Rothberg LJ. 2000. *Proc. Natl. Acad. Sci. USA* 97:11187–91
62. Paesler MA, Moyer PJ. 1999. *Near–Field Optics: Theory, Instrumentation and Applications.* New York: Wiley
63. Blatchford JW, Gustafson TL, Epstein AJ, Vanden Bout DA, Kerimo J, et al. 1996. *Phys. Rev. B* 54:3683–86
64. DeAro JA, Weston KD, Buratto SK, Lemmer U. 1997. *Chem. Phys. Lett.* 277:532–38
65. Teetsov J, Vanden Bout DA. 2002. *Langmuir* 18:897–903
66. McNeill JD, O'Connor DB, Adams DM, Barbara PF, Kammer SB. 2001. *J. Phys. Chem.* 105:76–82
67. Wei PK, Lin YF, Fann WS, Lee YZ, Chen SA. 2001. *Phys. Rev. B* 6304:U501–4
68. Nguyen T-Q, Schwartz BJ, Schaller RD, Johnson JC, Lee LF, et al. 2001. *J. Phys. Chem. B* 105:5153–60

69. McBranch DW, Kraabel B, Xu S, Kohlman RS, Klimov VI, et al. 1999. *Synth. Met.* 101:291–94
70. Klimov VI, McBranch DW. 1998. *Phys. Rev B* 58:7654–62
71. Denton GJ, Tessler N, Stevens MA, Friend RH. 1999. *Synth. Met.* 102:1008–9
72. Dogariu A, Vacar D, Heeger AJ. 1998. *Phys. Rev. B* 58:10218–24
73. Lim SH, Bjorklund TG, Gaab KM, Bardeen CJ. 2002. *J. Chem. Phys.* 117: 454–61
74. Frolov SV, Liess M, Lane PA, Gellerman W, Vardeny ZV, et al. 1997. *Phys. Rev. Lett.* 78:4285–88
75. Kepler RG, Valencia VS, Jacobs SJ, McNamara JJ. 1996. *Synth. Met.* 78:227–30
76. Haugeneder A, Hilmer M, Kallinger C, Perner M, Epstein AJ. 1998. *Appl. Phys. B* 66:389–92
77. Maniloff ES, Klimov VI, McBranch DW. 1997. *Phys. Rev. B* 756:1876–81
78. Hide F, Díaz-García MA, Schwartz BJ, Heeger AJ. 1996. *Science* 273:1833–36
79. Tessler N, Denton GJ, Friend RH. 1996. *Nature* 382:695–97
80. Frolov SV, Vardeny ZV, Yoshino K. 1998. *Phys. Rev. B* 57:9141–47
81. Long X, Grell M, Malinowski A, Bradley DDC. 1998. *Opt. Mater.* 9:70–76
82. Doan V, Tran V, Schwartz BJ. 1998. *Chem. Phys. Lett.* 288:576–84
83. Sluch MI, Pearson C, Petty MC, Halim M, Samuel IDW. 1998. *Synth. Met.* 94:285–89
84. Kim J, Swager TM. 2001. *Nature* 411: 1030–34
85. Schroder R, Heflin JR, Wang H, Gibson HW, Graupner W. 2001. *Synth. Met.* 121:1521–24
86. Durstock MF, Taylor B, Spry RJ, Chiang L, Reulbach S, et al. 2001. *Synth. Met.* 116:373–77
87. Shi Y, Liu J, Yang Y. 2000. *J. Appl. Phys.* 87:4254–63
88. Liu J, Guo TF, Shi YJ, Yang Y. 2001. *J. Appl. Phys.* 89:3668–73
89. Nguyen T-Q, Kwong RC, Thompson ME, Schwartz BJ. 2000. *Appl. Phys. Lett.* 76: 2454–56
90. Lee T-W, Park OO, Do LM, Zyun T. 2001. *Synth. Met.* 117:249–51
91. Lee T-W, Park OO. 2000. *Adv. Mater.* 12: 801–4
92. Reichardt C. 1979. *Solvent Effects in Organic Chemistry.* Weinheim: Verlag Chemie
93. Schaller RD, Lee LF, Johnson JC, Haber LH, Saykally RJ, et al. 2002. *J. Phys. Chem. B.* 106:9496–506
94. Wong KF, Skaf MS, Yang CY, Rossky PJ. 2001. *J. Phys. Chem. B* 105:6103–7
95. Lee JI, Klaemer G, Miller RD. 1999. *Chem. Mater.* 11:1083–88
96. Papadimitrakopoulos F, Yan M, Rothberg LJ, Katz HE, Galvin ME, et al. 1994. *Mol. Cryst. Liq. Cryst.* 256:663–69
97. Schaller RD, Johnson JC, Wilson KR, Lee LF, Haber LH, Saykally RJ. 2002. *J. Phys. Chem. B* 106:5143–54
98. Schaller RD, Snee PT, Johnson JC, Lee LF, Wilson KR, et al. 2002. *J. Chem. Phys.* 117:6688–98
99. Chen LH, McBranch DW, Wang HL, Helgeson R, Wudl F, Whitten DG. 1999. *Proc. Natl. Acad. Sci. USA* 96:12287–92
100. Stork M, Gaylord BS, Heeger AJ, Bazan GC. 2002. *Adv. Mater.* 14:361–66
101. Nguyen T-Q, Wu J, Doan V, Schwartz BJ, Tolbert SH. 2000. *Science* 288:652–55
102. Nguyen T-Q, Wu J, Tolbert SH, Schwartz BJ. 2001. *Adv. Mater.* 13:609–11
103. Schwartz BJ, Nguyen T-Q, Wu J, Tolbert SH. 2001. *Synth. Met.* 116:35–40
104. Tolbert SH, Firouzi A, Stucky GD, Chmelka BF. 1997. *Science* 278:264–67
105. Wu J, Gross AF, Tolbert SH. 1999. *J. Phys. Chem. B* 103:2374–84
106. Tolbert SH, Wu J, Gross AF, Nguyen T-Q, Schwartz BJ. 2001. *Microporous Mesoporous Mater.* 44:445–51
107. Lee J-I, Zyung T, Miller RD, Kim YH,

Jeoung SC, Kim D. 2000. *J. Mater. Chem* 10:1547–50
108. Scott JC, Brock PJ, Salem JR, Ramos S, Malliaras GG, et al. 2000. *Synth. Met.* 111:289–93
109. Hsieh BR, Yu Y, Forsythe EW, Schaaf GM, Feld WA. 1998. *J. Am. Chem. Soc.* 120:231–32
110. Halim M, Pillow JNG, Samuel IDW, Burn PL. 1999. *Synth. Met.* 102:922–23
111. Parker ID, Cao Y, Yang CY. 1999. *J. Appl. Phys.* 85:2441–47